Chem. Chem. Technol., 2025,
Vol. 19, No. 3, pp. 511–519

Chemical Technology

HYDRODYNAMICS OF CRUSHED OREGANO FILTRATION DRYING

***Alina Denysiuk*[1,✉], *Volodymyr Atamanyuk*[1], *Zoriana Hnativ*[1]**

https://doi.org/10.23939/chcht19.03.511

Abstract. The study presents the results of research into the hydrodynamics of gas flow filtration through a quasi-stationary layer during the filtration drying of crushed oregano, a pharmaceutical industry waste product remaining after the extraction of target components, as a raw material for the production of alternative solid fuel. The main geometric parameters of individual crushed oregano particles, as well as the physico-mechanical properties of the layer that settles under the influence of pressure drop, were determined experimentally. The experimental setup diagram is also provided.

An analytical method was used to determine the influence of layer height settlement, changes in the equivalent diameter of channels between particles, and layer porosity on pressure losses during gas flow percolation.

The results of the experimental studies are presented as functional dependencies: pressure loss $\Delta P = f(v_0)$, changes in the equivalent channel diameter $d_e = f(v_0)$, and layer porosity $\varepsilon = f(v_0)$ as functions of the apparent gas filtration velocity. The feasibility of preparing crushed oregano for the production of feed yeast, alternative solid fuel, etc., is substantiated.

The obtained results enable the prediction of energy consumption in the design of filtration drying equipment for crushed oregano.

Keywords: oregano, filtration drying, hydrodynamics, pressure loss, quasi-stationary layer.

1. Introduction

The pharmaceutical industry extensively uses raw materials of plant origin.[1] It is well known that oregano (*Origanum vulgare*) possesses a wide range of medicinal properties and serves as a source of biologically active components such as thymol, cymol, free alcohols, tannins, alkaloids, and ascorbic acid.[2] In pharmaceutical production, ethanol extraction is commonly used[3] to isolate valuable components from oregano leaves and stems. However, this process generates a significant amount of crushed oregano waste.

There are several ways to use this waste, including the production of feed yeast and alternative energy sources. Oregano's chemical composition includes numerous beneficial components such as vitamins A, B, and C, various organic acids, and other biologically active compounds. To enhance poultry production, compound feed with a balanced protein content is widely used. As reported, plant-based waste is currently considered the most suitable raw material for protein feed production. In Ukraine, the pharmaceutical industry waste amounts to nearly one million tons per year.[4] Due to the high moisture content of crushed oregano after the extraction of target products, its secondary use is limited. In most cases, it is disposed of in landfills.

Therefore, this study focuses on crushed oregano (CO) remaining after the extraction of its target components. A literature review indicates that developing efficient methods for the rational utilization of pharmaceutical waste is a relevant and pressing issue.

One of the potential solutions is using CO for the production of feed yeast or solid, environmentally friendly fuel. The global population growth is driving an increasing demand for green, sustainable energy. Biofuel is a stable and eco-friendly energy source for many countries. As an organic raw material, oregano contains approximately 30% lignocellulose and up to 50% cellulose,[5,6] making it a reliable natural source for alternative energy production. However, not only the chemical composition but also the physicochemical properties of biomass influence the quality of alternative solid fuels.[7] The moisture content of biomass[8] affects the lower heating value of biofuel combustion. Given that the moisture content of CO after extraction is 50–60% by mass, drying is a key stage in its preparation for use as biofuel.[9] According to recommendations from various authors,[10] the moisture content of natural biomass for briquetting should be in the range of 7–14%.

[1] Lviv Polytechnic National University, 12 Bandera Sr., Lviv 79013, Ukraine
✉ *alina.r.denysiuk@lpnu.ua*

Drying is one of the most energy-intensive processes in the chemical industry.[11] Based on the analysis of data,[12] filtration drying is considered one of the most efficient methods for drying crushed solid materials. Filtration drying[13] involves the percolation of a gas flow through a stationary layer of porous material under a pressure drop. One of the key characteristics determining the feasibility and efficiency of the selected drying method is the specific energy consumption required to create a pressure drop. Hydrodynamic studies allow for the prediction of these energy expenditures.

A study[14] investigated the hydrodynamics of filtration drying in cotton fiber, presenting dependencies for predicting pressure losses in a quasi-stationary cotton fiber layer, which exhibits settling behavior under a pressure drop. The study[15] presents the results of hydrodynamics research on the quasi-stationary layer of post-alcohol bard during filtration drying. The prediction of pressure losses in these studies is provided in the form of dimensionless complexes. Each material is characterized by different physico-mechanical properties (such as shape, size, equivalent diameter of channels between particles in the layer, porosity, bulk density, *etc*.). Therefore, it is impossible to apply calculation dependencies or criterion equations obtained by other authors for the materials they studied. This is due to the lack of a unified approach to averaging the sizes of irregularly shaped particles, which leads to significant discrepancies between experimental data and theoretically determined values calculated using existing dependencies.

2. Experimental

2.1. Materials

The object of study was the waste from the pharmaceutical industry – crushed oregano remaining after ethanol extraction. Crushed oregano consists of flat particles, where the width and length of these particles are significantly greater than their thickness. The geometric dimensions of the crushed oregano particles (width and length) were determined by measuring with an electronic caliper model VOREL 150 mm (resolution of 0,1 mm, accuracy ±0,2 mm), while the thickness of the particles was measured using an electron microscope model MBB-1A. More than 200 samples of crushed oregano particles were analyzed. The crushed oregano consisted of flat particles with a length of 2-5,5 mm, a width of 3-5 mm, and a thickness of 0,14-0,16 mm (Fig. 1). The true density was determined by compressing the oregano particles, reduced to a size of no more than 0,0001 mm. This allowed the determination of the mass and volume of the oregano without pores or cracks. The bulk density of the oregano was determined according to the method outlined in DSTU ISO 567-2002. The apparent density was calculated using the previously measured geometric dimensions of the particles. The true density of the oregano was 1470 kg/m³, the bulk density was 223 kg/m³, and the apparent density was 740 kg/m³. The porosity of the layer was determined using the two-liquid method and was found to be 0.3515 m³/m³.

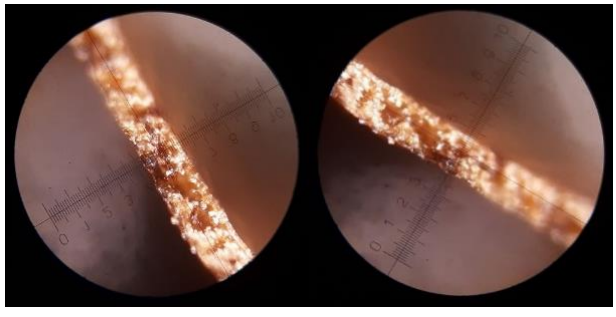

Fig. 1. Measurement of the oregano particle thickness using the MBB-1A microscope

The average particle sizes were determined as the mean value for each particle dimension. The percentage composition of particles of each size was determined by weighing using an AXIS-AD3000 scale (with a measurement accuracy of 0,01 g). The determined average geometric dimensions of the particles are presented in Table 1.

Table 1. Geometric characteristics of CO

Average Linear Dimensions, m			External Surface Area, $S \cdot 10^5$, m²	Volume, $V \cdot 10^9$, m³
Length, $a \cdot 10^3$, m	Width, $b \cdot 10^3$, m	Thickness, $c \cdot 10^3$, m		
3.59	4.17	0.15	3.22	2.37

2.2. Methods

The study of the hydrodynamics of gas flow through a quasi-stationary CO layer was conducted using an experimental setup shown in Fig. 2. It was established that the CO waste layer settles under the application of a pressure drop. Therefore, all experimental studies were carried out using appropriate CO sample weights.

The setup consists of a CO container (4) mounted on a receiver (6). Inside the container, a ruler is placed to measure the change in layer height during the application of a pressure drop (Fig. 3). The receiver is connected to a vacuum pump (7) through pipelines, a rotameter PF 20-200-LPH (2), a shut-off valve (1), and a regulating valve (5). The pressure drop difference was measured using a vacuum gauge WK 688 L (3).

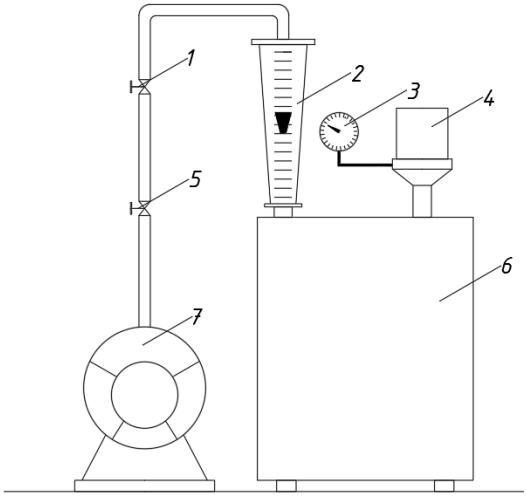

Fig. 2. Diagram of the setup for determining pressure losses in the quasi-stationary CO layer: 1 – shut-off valve; 2 – rotameter PF 20-200-LPH; 3 – vacuum gauge WK 688 L; 4 – CO waste container; 5 – regulating valve; 6 – receiver; 7 – vacuum pump

For the experiment, the required CO sample weight was placed into container 4 and set on receiver 6. After activating vacuum pump 7, regulating valve 5 was used to control the gas flow rate passing through the CO layer. The gas flow rate was measured with rotameter 2, while pressure losses in the quasi-stationary layer were recorded using vacuum gauge 3.

The layer height variation was measured using ruler 1. Each material sample was tested at least three times, with a fresh portion of CO used for each experiment. A minimum of ten height measurements were taken. The weight of each material portion was determined using an AXSIS-3000 electronic scale (accuracy ±0,01 g). The initial bulk density and initial layer height were consistent across all experiments.

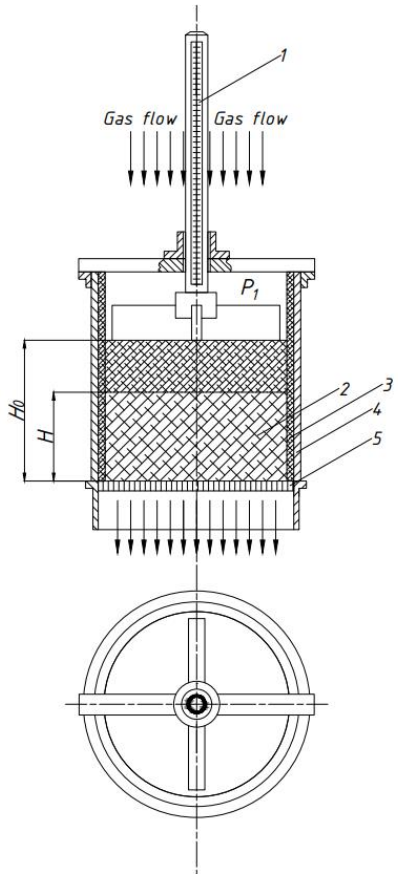

Fig. 3. Diagram of the experimental container: 1 – ruler; 2 – quasi-stationary CO waste layer; 3 – thermal insulation insert; 4 – base of the experimental container; 5 – perforated partition

As mentioned earlier, the height of the CO layer depends on the pressure drop, meaning that as the pressure drop increases, the layer height decreases. As a result, several parameters of the quasi-stationary layer change, including its porosity, the equivalent diameter of the channels between CO particles, and the actual velocity of the gas flow through the particles. An increase in the actual gas filtration velocity υ leads to higher pressure losses ΔP in the layer, while a decrease in layer height results in an increase in its bulk density ρ_b. The only parameters that remain constant are the material mass in the container and the total surface area of all particles. Thus, the following functional dependencies can be established:

$$H = f(\upsilon);\ d_e = f(\upsilon);\ \rho_b = f(\upsilon);\ \varepsilon = f(\upsilon);$$

$$\Delta P = f(\upsilon);\ F = const;\ G = const.$$

The well-known Darcy-Weisbach[16] equation is used to determine pressure losses in the quasi-stationary porous CO layer. This equation describes the impact of all the previously mentioned process parameters on pressure losses:

$$\Delta P = \lambda \cdot \frac{H}{d_e} \cdot \frac{\rho \cdot v_0^2}{2}, \quad (1)$$

where ΔP is a pressure drop in the layer, Pa; λ is a hydraulic friction coefficient; H is a current layer height of CO, m; d_e is the current equivalent diameter of the channels, m; ρ is gas flow (air) density, kg/m³; v_0 is an apparent velocity of the gas flow, m/s.

The equivalent diameter of the channels d_e was determined using the following equation:

$$d_e = \frac{4 \cdot \varepsilon}{a}, \quad (2)$$

where ε is a current porosity of the stationary material layer, m³/m³; a is the specific surface area of all particles in the quasi-stationary layer of crushed oregano, m²/m³.

As noted above, due to the settling of the oregano layer, the equivalent diameter of the channels between the particles and the specific surface area change, which is why this layer is referred to as a quasi-stationary layer. The initial specific surface area of the particles in the oregano layer a_0 was calculated using the following equation:

$$a_0 = \frac{F}{H_0 \cdot S}, \quad (3)$$

where H_0 is the initial height of the CO layer, m; S is the cross-sectional area of the container, m².

If we assume that the container contains N identical CO particles, the external surface area F of all the flat particles can be expressed as follows:

$$F = 2 \cdot (a \cdot b + a \cdot c + b \cdot c) \cdot N, \quad (4)$$

where a, b, c are the averaged length, width, and thickness of the CO particles, respectively, m.

Given that the apparent density of oregano ρ_a and the averaged particle sizes are known, the mass of the material in the container can be expressed by the following equation:

$$G = a \cdot b \cdot c \cdot N \cdot \rho_a, \quad (5)$$

From this, the number of particles N in the quasi-stationary layer can be determined:

$$N = \frac{G}{a \cdot b \cdot c \cdot \rho_a}. \quad (6)$$

The initial specific surface area a_0, for the initial height H_0 of the CO layer, is calculated as the ratio of the total surface area of all the particles to the volume they occupy:

$$a_0 = \frac{2 \cdot (a \cdot b + a \cdot c + b \cdot c) \cdot G}{a \cdot b \cdot c \cdot \rho_a \cdot S \cdot H_0}, \quad (8)$$

Thus, the current specific surface area can be expressed by the following equation:

$$a = a_0 \cdot \frac{H_0}{H}, \quad (9)$$

where a_0 and a are the initial and current specific surface areas of the CO layer, m²/m³;

Considering the above, the current specific surface area was determined using the following equation:

$$a = \frac{2 \cdot (a \cdot b + a \cdot c + b \cdot c) \cdot G}{a \cdot b \cdot c \cdot \rho_a \cdot S \cdot H_0} \cdot \frac{H_0}{H} = \frac{2 \cdot (a \cdot b + a \cdot c + b \cdot c) \cdot G}{a \cdot b \cdot c \cdot \rho_a \cdot S \cdot H}, \quad (10)$$

The mass of the material layer can be expressed through its true density as follows:

$$G = h_t \cdot \rho_t \cdot S, \quad (11)$$

where h_t is the height of the CO layer with density ρ_t, m.

Then:

$$a = \frac{2 \cdot (a \cdot b + a \cdot c + b \cdot c) \cdot h_t \cdot \rho_t \cdot S}{a \cdot b \cdot c \cdot \rho_a \cdot S \cdot H} = \frac{2 \cdot (a \cdot b + a \cdot c + b \cdot c) \cdot h_t \cdot \rho_t}{a \cdot b \cdot c \cdot \rho_a \cdot H}, \quad (12)$$

The pressure losses, based on Eq. (1) and considering Eq. (2), can be expressed by the following equation:

$$\Delta P = \lambda \cdot \frac{H \cdot a}{4 \cdot \varepsilon} \cdot \frac{\rho \cdot v_0^2}{2}. \quad (13)$$

Since the hydraulic resistance coefficient of the layer λ is dependent on the Reynolds number, then:

$$\lambda = \frac{A}{Re} + B = A \cdot \frac{\mu \cdot \varepsilon \cdot a}{4 \cdot \varepsilon \cdot v_0 \cdot \rho} + B. \quad (14)$$

Then, Eq. (1) can be written as follows:

$$\Delta P = A \cdot \frac{\mu \cdot a^2 \cdot H \cdot v_0}{32 \cdot \varepsilon^3} + B \cdot \frac{H \cdot a \cdot \rho \cdot v_0^2}{8 \cdot \varepsilon^3}, \quad (15)$$

where A and B are unknown coefficients determined experimentally; μ is the dynamic viscosity coefficient of air, Pa·s.

Eq. (15) can be rewritten as a linear equation:

$$\frac{\Delta P \cdot \varepsilon^3}{a^2 \cdot H \cdot v_0} = A^* + B^* \cdot \frac{v_0}{a}, \quad (16)$$

where $A^* = A \cdot \frac{\mu}{32}$, and $B^* = B \cdot \frac{\rho}{8}$.

Once the unknown coefficients A* and B* are determined, Eq. (16) can be used to predict the pressure loss during the filtration drying of CO waste.

3. Results and Discussion

The main parameters of the layer for each sample of CO are represented in Table 2.

As a result of the experiments, a functional dependence between the pressure drop and the apparent velocity, $\Delta P = f(v_0)$, was established, as illustrated in Fig. 4.

Table 2. Characteristics of the quasi-stationary layer of crushed CO

Sample mass, G, kg	Initial porosity of the layer, ε_0, m^3/m^3	Surface area of all CO particles, F, m^2	Height of the CO layer H_0, with density ρ_b, m
0.06	0.3497	548608	0.0355
0.1	0.3511	914347	0.0595
0.15	0.3500	1371520	0.089
0.185	0.3502	1691541	0.11
0.24	0.3496	2194432	0.1425

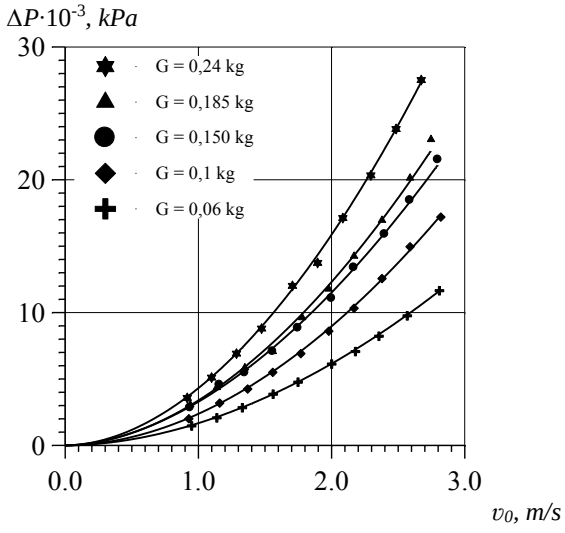

Fig. 4. Dependence of pressure loss in the quasi-stationary layer of CO on the apparent filtration velocity of the gas flow for different material samples

By analyzing Fig. 4, we can conclude that the curves exhibit a parabolic shape. This suggests that both inertial and viscous components affect the pressure loss in the quasi-stationary layer of CO. Fig. 5 presents the variation in the equivalent diameter of the channels for all CO samples as the apparent filtration velocity of the gas flow through the CO layer changes $de = f(v_0)$.

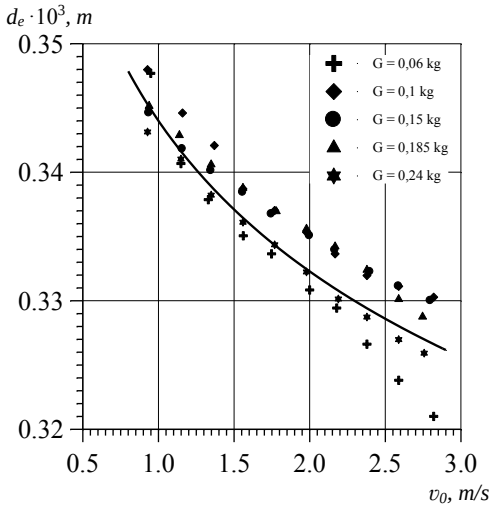

Fig. 5. Dependence of the equivalent diameter of the channels between CO particles on the apparent filtration velocity of the gas flow

As the equivalent diameter of the channels and the apparent velocity change, the porosity of the CO layer also varies. The dependence of the porosity of the layer for all CO samples on the apparent velocity $\varepsilon = f(v_0)$ is shown in Figs 6 and 7.

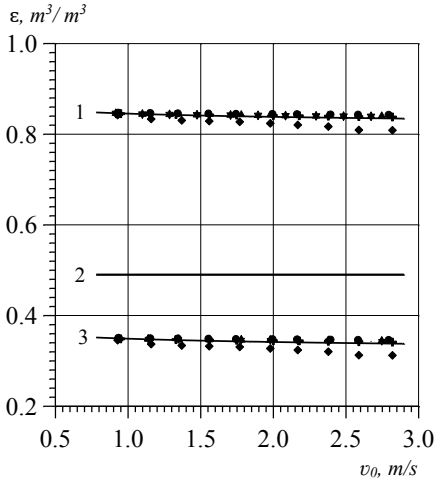

Fig. 6. Graph showing the dependence of the porosity change in the quasi-stationary layer on the apparent filtration velocity of the gas flow: 1 – total porosity; 2 – internal porosity; 3 – layer porosity

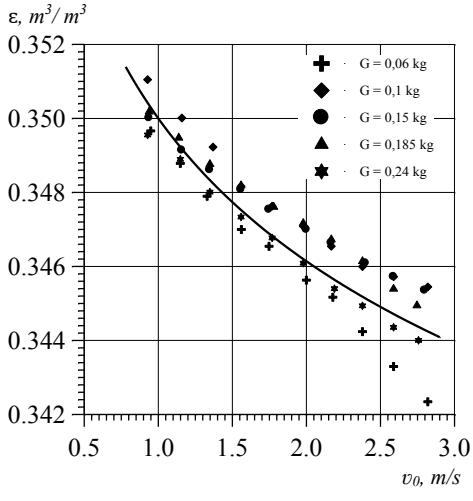

Fig. 7. Dependence of the change in the porosity of the CO layer on the apparent filtration velocity of the gas flow

After performing an approximation of the experimental data (Figs 5 and 7) for the change in the height of the quasi-stationary CO layer using a power function, the dependencies for calculating the running values of the equivalent diameter and porosity of the layer were obtained:

$$d_e = 0{,}344 \cdot v_0^{-0{,}05} \quad (17)$$

$$\varepsilon = 0{,}35 \cdot v_0^{-0{,}016} \quad (18)$$

The results of the experimental studies were summarized in the form of a graphical dependence shown in Fig. 8.

After performing a linear approximation of the experimental data over the segment intercepting the ordinate axis, the value $A^* = A \cdot \frac{\mu}{32}$, was determined, while the value $B^* = B \cdot \frac{\rho}{8}$ was obtained using the tangent of the slope angle. The Eq. (16) then takes the following form:

$$\frac{\Delta P \cdot \varepsilon^3}{a^2 \cdot H \cdot v_0} = 2{,}5 \cdot 10^{-5} + 0{,}223 \cdot \frac{v_0}{a}. \quad (19)$$

This dependence can be used to predict pressure losses during the filtration drying of CO. Fig. 9 shows a comparison of experimental data with the theoretically calculated values.

The comparison of the experimentally obtained values of the equivalent diameter of the channels with the theoretical values calculated using dependence (17) is shown in Fig. 9 a. Fig. 9 b illustrates the comparison of the experimental and theoretical values of the porosity of the CO layer calculated using dependence (18). In Fig. 9 c, the comparison of the experimental values of pressure losses in the quasi-stationary CO layer with the theoretical values calculated using dependence (19) is presented. The maximum relative accuracy between the experimental and theoretical values is within 11%.

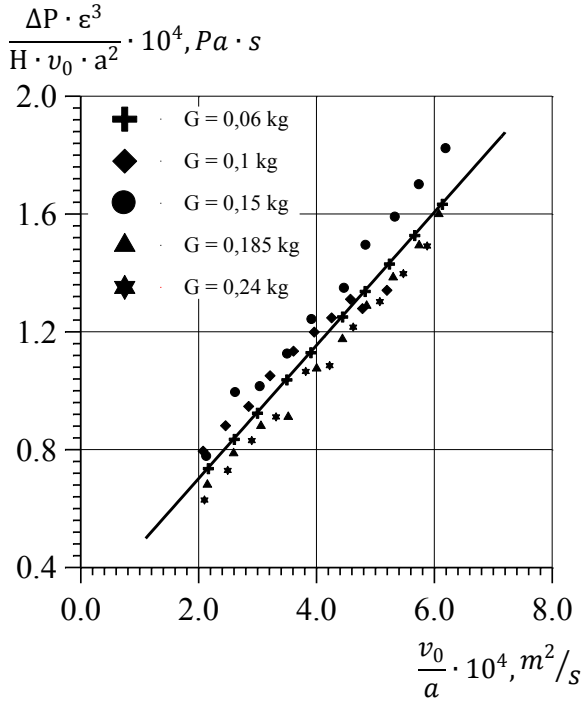

Fig. 8. Dependence $\frac{\Delta P \cdot \varepsilon^3}{H \cdot v_0 \cdot a^2} = f\left(\frac{v_0}{a}\right)$ for the crushed oregano

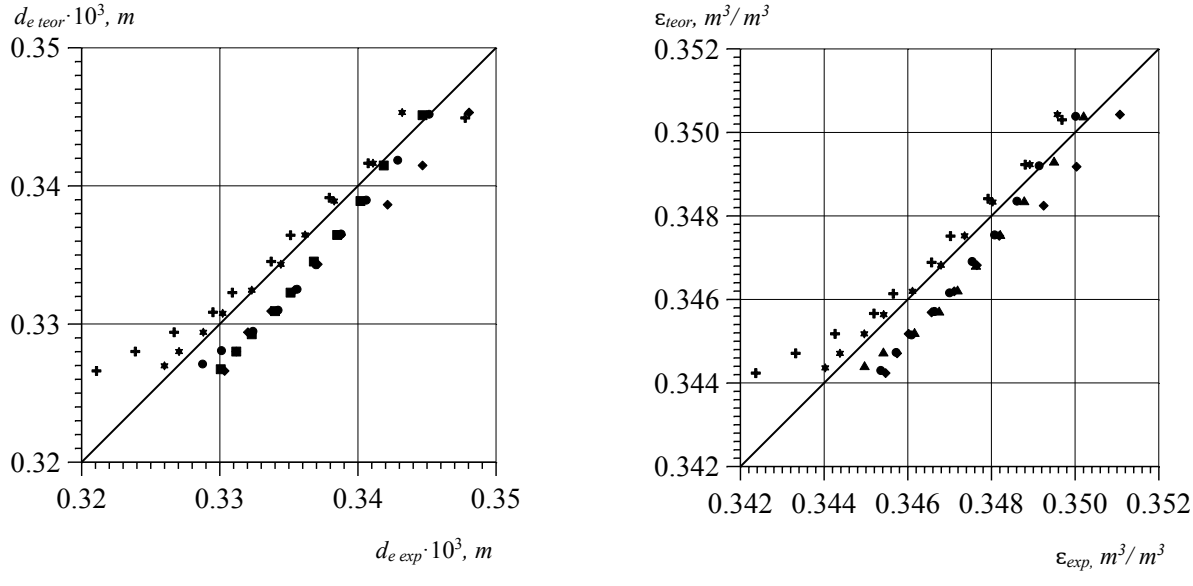

Fig. 9. Dependence between experimental data and theoretically calculated values: a) according to Eq. (17); b) according to Eq. (18) (the notations correspond to those in Fig. 4)

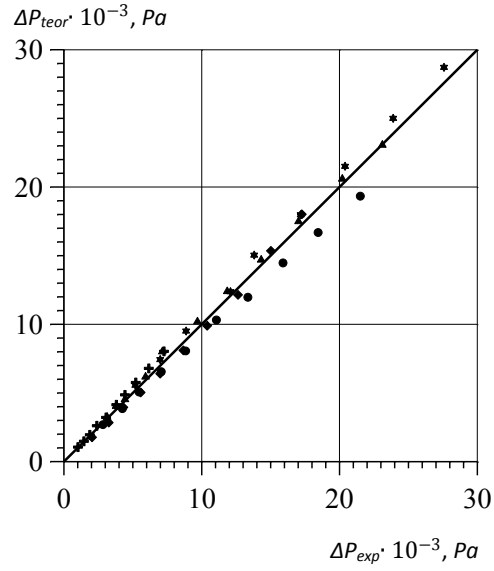

Fig. 9. Dependence between experimental data and theoretically calculated values: c) according to Eq. (19) (the notations correspond to those in Fig. 4)

To use the results of experimental studies on the hydrodynamics of gas flow filtration through a quasi-stationary layer of crashed oregano, for predicting energy costs associated with creating pressure drops in industrial installations of various geometrical sizes and different productivity, the obtained results should be presented in the form of dimensionless complexes, that is, as a dependence of the Euler number on the equivalent Reynolds number (Fig. 12).

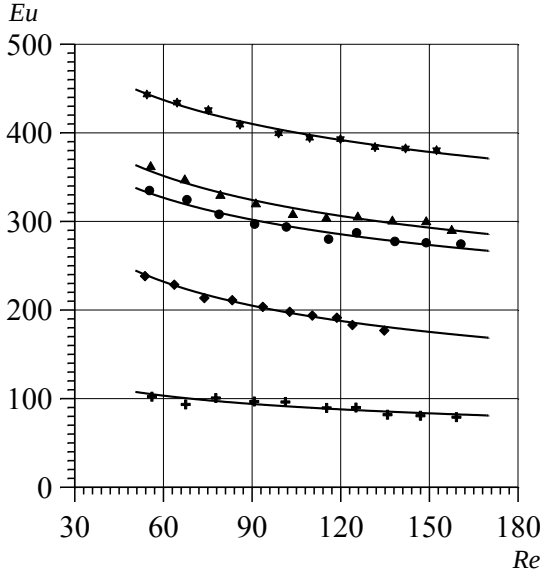

Fig. 12. Dependence of the Euler number on the Reynolds number (notations are according to Fig. 4)

The value of the Euler number was calculated using the formula:

$$Eu = \frac{\Delta P}{(\rho \cdot v^2)}. \quad (20)$$

The equivalent value of the Reynolds number was determined using the dependence:

$$Re = \frac{v \cdot d_e \cdot \rho}{\mu}. \quad (21)$$

Analysis of Fig. 12 shows that the Euler number depends not only on the Reynolds number but also on the mass of the sample, *i.e.*, the current height of the CO layer. By approximating the experimental data with a power function, the calculation dependencies *Eu = f(Re)* were obtained. The results are presented in Table 3.

Table 3. Calculation dependencies of the Euler number for different samples of crashed oregano

G, kg	Eu
0.06	$Eu = 430 \cdot Re^{-0,22}$
0.1	$Eu = 615 \cdot Re^{-0,22}$
0.15	$Eu = 795 \cdot Re^{-0,22}$
0.185	$Eu = 870 \cdot Re^{-0,22}$
0.240	$Eu = 1110 \cdot Re^{-0,22}$

Therefore, the Euler number can be represented as a calculated dependence:

$$Eu = \mathrm{A} \cdot Re^{-\mathrm{x}}, \quad (22)$$

where A is a coefficient that depends on the sample of the material, *i.e.*, the current height of the layer, and it can be represented as:

$$\mathrm{A} = f\left(\frac{H_e}{d_e}\right), \quad (23)$$

where $H_e = 1{,}5 \cdot \mathrm{H}$, since the gas flow moves through the curved channels of the quasi-stationary layer between the particles of the CO.

As observed, the exponent near the Reynolds number remains constant, while the coefficient *A* depends on the sample mass of CO, meaning it is influenced by the current height of the layer. To generalize all the studied samples, the functional dependence of the Euler number on the geometric simplex (H_e/d_e) is shown in Fig. 13.

The approximation of experimental data using a power function allowed to obtain a generalized dependence for determining the Euler number:

$$Eu = 14 \cdot Re^{-0,22} \cdot \left(\frac{H_e}{d_e}\right)^{0,67}. \quad (24)$$

This dependence is valid within the Reynolds number range of $40 \leq Re \leq 180$.

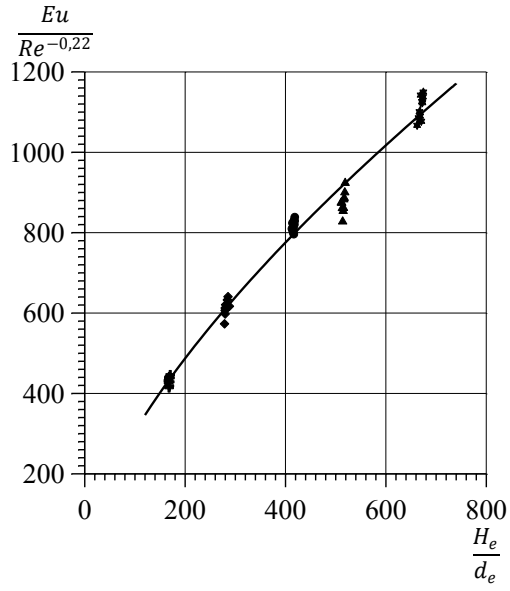

Fig. 13. Dependence of the Euler number on the geometric simplex (H_e/d_e) (notations according to Fig. 4)

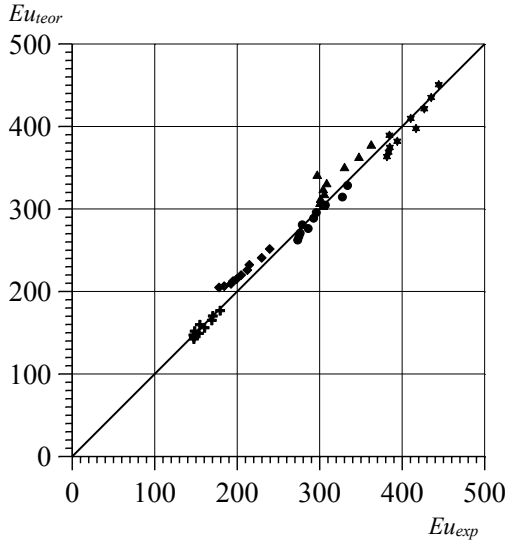

Fig. 14. Comparison of Euler number values calculated theoretically and obtained experimentally (notations according to Fig. 4)

According to Fig. 14, the absolute value of the maximum relative accuracy between the values of the Euler number calculated from experimental data and those obtained from Eq. (24) does not exceed 7.9%.

4. Conclusions

This study investigates for the first time the internal hydrodynamics of the quasi-stationary layer of crushed oregano particles, a byproduct of the pharmaceutical industry, which exhibits settling behavior when a pressure difference is applied. It has been established that changes in the height of the quasi-stationary layer lead to changes in the equivalent diameter of the channels through which the gas flow is filtered, the porosity of the layer, and the active specific surface it interacts with. Given that the particles of crushed oregano possess internal porosity, derived calculation dependencies were developed to determine the change in the equivalent diameter of the channels between particles and, accordingly, the specific surface area of the crushed oregano particles. Unknown coefficients of the Darcy-Weisbach equation, A^* and B^*, were determined for predicting pressure losses in the quasi-stationary layer of CO, and the dependence of the Euler number on the Reynolds number was established for all CO samples. A comparison was made between the theoretically calculated data, obtained from dependencies (17), (18), (19), and (24), and the data obtained experimentally.

References

[1] Esparza, I.; Jiménez-Moreno, N.; Bimbela, F.; Ancín-Azpilicueta, C.; Gandía, L. M. Fruit and Vegetable Waste Management: Conventional and Emerging Approaches. *J. Environ. Manage.* 2020, *265*, 110510. https://doi.org/10.1016/j.jenvman.2020.110510

[2] De Torre, M. P.; Vizmanos, J. L.; Cavero, R. Y.; Calvo, M. I. Improvement of Antioxidant Activity of Oregano (Origanum vulgare L.) with an Oral Pharmaceutical Form. *Biomed. Pharmacother.* 2020, *129*, 110424. https://doi.org/10.1016/j.biopha.2020.110424

[3] Jafari Khorsand, G.; Morshedloo, M. R.; Mumivand, H. Natural Diversity in Phenolic Components and Antioxidant Properties of Oregano (Origanum vulgare L.) Accessions, Grown under the Same Conditions. *Sci. Rep.* 2022, *12*, 5813. https://doi.org/10.1038/s41598-022-09742-4

[4] Kylymenchuk, O.; Velichko, T.; Malovanyy, M.; Umanets, A.; Hnilichenko, A.; Lahotska, A. Non-Traditional Raw Materials for Biotechnological Industries and Some Environmental Aspects of Their Disposal. *Food Sci. Technol.* 2020, *14*, 32–38. https://doi.org/10.15673/fst.v14i1.1652

[5] Rajendran, N.; Gurunathan, B.; Han, J.; Krishna, S.; Ananth, A.; Venugopal, K.; Priyanka, R. S. Recent Advances in Valorization of Organic Municipal Waste into Energy Using Biorefinery Approach, Environment and Economic Analysis. *Bioresour. Technol.* 2021, *337*, 125498. https://doi.org/10.1016/j.biortech.2021.125498

[6] Jha, S.; Okolie, J. A.; Nanda, S.; Dalai, A. K. A Review of Biomass Resources and Thermochemical Conversion Technologies. *Chem. Eng. Technol.* 2022, *45*, 791–799. https://doi.org/10.1002/ceat.202100503

[7] Knapczyk, A.; Francik, S.; Fraczek, J.; Slipek, Z. Analysis of Research Trends in Production of Solid Biofuels. *Eng. Rural Dev.* 2019, *18*, 1503–1509. https://doi.org/10.22616/ERDev2019.18.N415

[8] Angulo-Mosquera, L. S.; Alvarado-Alvarado, A. A.; Rivas-Arrieta, M. J.; Cattaneo, C. R.; Rene, E. R.; García-Depraect, O. Production of Solid Biofuels from Organic Waste in Developing

Countries: A Review from Sustainability and Economic Feasibility Perspectives. *Sci. Total Environ.* 2021, *795*, 148816. https://doi.org/10.1016/j.scitotenv.2021.148816
[9] Zhou, C.; Fan, X.; Duan, C.; Zhao, Y. A Method to Improve Fluidization Quality in Gas–Solid Fluidized Bed for Fine Coal Beneficiation. *Particuology* 2019, *43*, 181–192. https://doi.org/10.1016/j.partic.2017.12.012
[10] Guibunda, F. A.; Waita, S.; Nyongesa, F. W.; Snyder, G. J.; Chaciga, J. Optimizing Biomass Briquette Drying: A Computational Fluid Dynamics Approach with a Case Study in Mozambique. *Energy* 2024, *360*, 100012. https://doi.org/10.1016/j.energ.2024.100012
[11] Potapov, V.; Yakushenko, Ye.; Grytsenko, O. Experimental Studies of the Kinetics of Temperature in Filtration Drying under Elevated Pressure. *Sci. Works* 2021, *85*, 2064. https://doi.org/10.15673/swonaft.v85i1.2064
[12] Mykychak, B.; Biley, P.; Kindzera, D. External Heat-and-Mass Transfer during Drying of Packed Birch Peeled Veneer. *Chem. Chem. Technol.* 2013, *7*, 191–195. https://doi.org/10.23939/chcht07.02.191
[13] Ivashchuk, O.; Atamanyuk, V.; Chyzhovych, R.; Manastyrska, V. A.; Barabakh, S. A.; Hnativ, Z. Kinetic Regularities of the Filtration Drying of Barley Brewer's Spent Grain. *Chem. Chem. Technol.* 2024, *18*, 66–75. https://doi.org/10.23939/chcht18.01.066
[14] Atamanyuk, V.; Gnativ, Z.; Kindzera, D.; Janabayev, D.; Khusanov, A. Hydrodynamics of Cotton Filtration Drying. *Chem. Chem. Technol.* 2020, *14*, 426–432. https://doi.org/10.23939/chcht14.03.426
[15] Ivashchuk, O.; Chyzhovych, R.; Atamanyuk, V. Simulation of the Thermal Agent Movement Hydrodynamics through the Stationary Layer of the Alcohol Distillery Stillage. *Case Stud. Chem. Environ. Eng.* 2024, *9*, 100566. https://doi.org/10.1016/j.cscee.2023.100566.
[16] Atamanyuk, V.; Huzova, I.; Gnativ, Z. Intensification of Drying Process during Activated Carbon Regeneration. *Chem. Chem. Technol*. 2018, *12*, 263–271. https://doi.org/10.23939/chcht12.02.263

Received: February 07, 2025 / Revised: May 11, 2025 / Accepted: June 03, 2025

ГІДРОДИНАМІКА ФІЛЬТРАЦІЙНОГО СУШІННЯ ПОДРІБНЕНОЇ МАТЕРИНКИ

Анотація. *У роботі наведено результати дослідження гідродинаміки профільтровування газового потоку крізь умовно стаціонарний шар під час фільтраційного сушіння подрібненої материнки – відходів фармацевтичної промисловості після екстрагування цільових компонентів як сировини для виготовлення альтернативного твердого палива. Експериментально визначено основні геометричні параметри окремих частинок подрібненої материнки, фізико-механічні властивості шару, який сідає під дією перепаду тисків. Також наведено схему експериментальної установки. Аналітичним методом було визначено вплив сідання висоти, зміни еквівалентного діаметру каналів між частинками та порізності шару на величину втрат тиску під час профільтровування газового потоку.*

Результати проведених експериментальних досліджень наведені у вигляді функціональних залежностей: втрати тиску $\Delta P = f(v_0)$, зміни еквівалентного діаметру каналів $d_e = f(v_0)$ та порізності шару $\varepsilon = f(v_0)$ від фіктивної швидкості фільтрування газового потоку. Обґрунтовано доцільність підготовки подрібненої материнки для виготовлення кормових дріжджів, альтернативного твердого палива тощо.

Завдяки отриманим результатам можна прогнозувати енергетичні витрати під час проектування обладнання фільтраційного сушіння подрібненої материнки.

Ключові слова: *материнка, фільтраційне сушіння, гідродинаміка, втрати тиску, умовно стаціонарний шар.*